Epimorphin$^{-/-}$ mice have increased intestinal growth, decreased susceptibility to dextran sodium sulfate colitis, and impaired spermatogenesis

Yuan Wang,[1] Lihua Wang,[1] Hristo Iordanov,[1] Elzbieta A. Swietlicki,[1] Qun Zheng,[1] Shujun Jiang,[1] Yuzhu Tang,[1] Marc S. Levin,[1,2] and Deborah C. Rubin[1,3]

[1]Department of Medicine and [2]Speciality Care Service Line, St. Louis VA Medical Center, St. Louis, Missouri, USA.
[3]Department of Molecular Biology and Pharmacology, Washington University School of Medicine, St. Louis, Missouri, USA.

Dynamic and reciprocal epithelial-mesenchymal interactions are critical for the normal morphogenesis and maintenance of epithelia. Epimorphin has been identified as a unique molecule expressed by mesenchymal cells and myofibroblasts and has putative morphogenetic effects in multiple epithelial tissues, including intestine, skin, mammary gland, lung, gallbladder, and liver. To define the in vivo role of epimorphin, we created epimorphin-null mice by targeted inactivation of the epimorphin gene. Male *epimorphin*$^{-/-}$ mice are sterile due to abnormal testicular development and impaired spermatogenesis. Intestinal growth is increased in *epimorphin*$^{-/-}$ mice due to augmented crypt cell proliferation and crypt fission during the neonatal (suckling) period, mediated at least in part by changes in bone morphogenetic protein (Bmp) and Wnt/β-catenin signaling pathways. Colonic mucosal injury and colitis induced by dextran sodium sulfate (DSS) are ameliorated in *epimorphin*$^{-/-}$ mice, probably due to the increased proliferative capacity of the *epimorphin*$^{-/-}$ colon. These in vivo findings support the notion that epimorphin is a key stromal regulator of epithelial cell proliferation and growth in the intestine. In addition, our studies demonstrate a novel and critical role for epimorphin in regulating testicular development and growth as well as spermatogenesis.

Introduction

Dynamic and reciprocal signaling between epithelium and mesenchyme is required for the growth and morphogenesis of epithelial tissues (1–3). ECM molecules, mesenchymal cell surface molecules, and soluble growth factors produced by mesenchyme regulate epithelial morphogenesis. Examples of mesenchymal factors include hepatocyte and fibroblast growth factors as well as members of the forkhead and bone morphogenetic protein (Bmp) molecule families, which regulate epithelial growth and promote morphogenesis and differentiation (4–6).

Epimorphin is a unique mesenchymal molecule that has morphogenetic effects in multiple epithelial tissues, including intestine, pancreas, mammary gland, lung, gallbladder, and liver (7–12), yet its precise in vivo functions remain unknown. We have shown that epimorphin is expressed in the mesenchyme of the developing fetal gut (13) and in intestinal myofibroblasts (14, 15), which form a subepithelial network that is in intimate contact with the crypt and villus epithelial cells. Epimorphin is most abundantly expressed in the fetal gut mesenchyme during villus morphogenesis, when mesenchymal cells invaginate into the undifferentiated endoderm and form small finger-like villus structures and proliferating cells become confined to the intervillus regions of the small and large bowels (the future crypts of Lieberkühn in the small bowel and colonic crypts in the large bowel) (16). Changes in the level of epimorphin expression by transfection of sense or antisense epimorphin constructs into myofibroblasts dramatically affects the morphology of cocultured epithelial cells (15). Inhibition of epimorphin expression promotes the growth and spreading of cocultured epithelial cells, and overexpression of epimorphin in myofibroblasts induces the formation of round epithelial colonies that develop small lumens. In addition, we showed that retinoic acid treatment of myofibroblasts derived from neonatal ileum upregulates epimorphin expression (14). These studies suggest that epimorphin might exert antiproliferative, promorphogenetic effects on adjacent epithelium. Our findings complement studies in skin, lung, mammary gland, colon, gallbladder, and pancreas that indicate that epimorphin is expressed in fibroblasts and myofibroblasts surrounding the epithelium (9). In each tissue, epimorphin has been postulated to function as a regulator of epithelial morphogenesis, promoting branching or the formation of ductular or luminal structures in these epithelia (12).

Epimorphin is a member of the syntaxin family of membrane-bound, intracellular vesicle-docking proteins (identical to rat syntaxin 2). These proteins are known as target membrane SNAREs (t-SNAREs). Monomeric epimorphin has been detected intracellularly as a component of the SNARE machinery that targets vesicles to the plasma membrane (17, 18). As such, it has been postulated to be involved in regulating the release of growth and/or morphogenetic factors by mesenchymal/myofibroblast cells (15). However, studies in the mammary gland have shown that dimeric and tetrameric epimorphin molecules are found on

Nonstandard abbreviations used: BAC, bacterial artificial chromosome; BMP, bone morphogenetic protein; DSS, dextran sodium sulfate; ISEMF, intestinal subepithelial myofibroblasts; Neo, loxP-flanked neomycin.

Conflict of interest: The authors have declared that no conflict of interest exists.

Citation for this article: *J. Clin. Invest.* **116**:1535–1546 (2006). doi:10.1172/JCI25442.

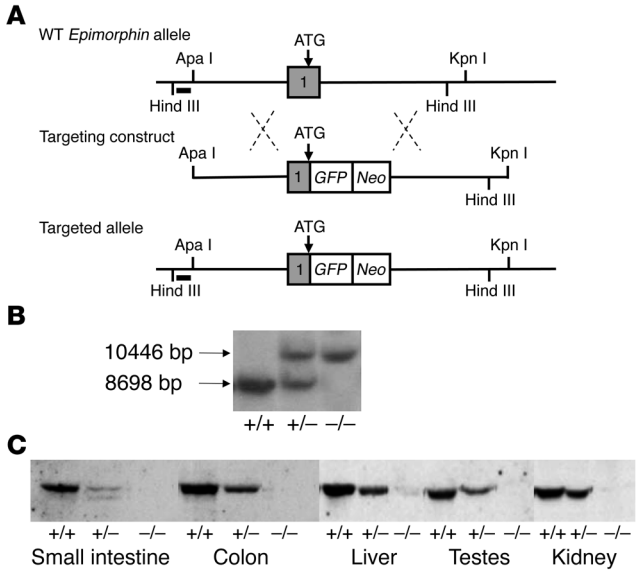

Figure 1
Generation and characterization of *epimorphin*$^{-/-}$ mice. (**A**) Targeting scheme to disrupt the *epimorphin* locus. Homologous recombination between the targeting vector and the WT allele produced the targeted allele in which 30 bp of the coding sequence in exon 1 and 1015 bp in intron 1 of the *epimorphin* gene were replaced by the coding sequence of enhanced GFP and a Neo cassette. The black bar represents the location of the probe used to identify targeted ES cell clones. The arrows denote the position of the initiator methionine of epimorphin and GFP. (**B**) Southern blot hybridization of Hind III–digested genomic DNA. A 10.4-kb band in the targeted allele and 8.7-kb band in the WT allele were produced as expected. (**C**) Immunoblot analysis of protein extracts from epimorphin WT (+/+), heterozygous (+/–), and null (–/–) mice. Total protein from small intestine, colon, liver, kidney, and testis (100 μg per tissue) was loaded onto the gel. Epimorphin was reduced in the tissues of heterozygous mice and absent in null mice.

the extracellular surface of stromal cells (7, 10) and thus are presumed to transmit signals by interacting with putative epithelial epimorphin receptors that have not yet been identified. Soluble monomeric and dimeric epimorphin molecules were also detected in dam's milk (10), suggesting that epimorphin might also act as a soluble factor in regulating epithelial morphogenesis.

Although previous data are consistent with a role for epimorphin in morphogenesis, the precise role of epimorphin in vivo is unclear. To clarify the physiological role(s) of epimorphin, *epimorphin*$^{-/-}$ mice were created by targeted inactivation of the *epimorphin* gene. The studies reported here present compelling evidence that epimorphin is a key mesenchymal factor regulating the proliferation of the intestinal epithelium and is essential for normal spermatogenesis and morphogenesis of the testis.

Results

Generation of epimorphin$^{-/-}$ *mice.* To study the in vivo role of epimorphin, *epimorphin*$^{-/-}$ mice were generated by targeted homologous recombination. The targeting construct was designed to replace the initiator methionine and coding sequence of *epimorphin* exon 1 with that of GFP and a loxP-flanked neomycin (Neo) cassette (Figure 1A). The generation of *epimorphin* heterozygous (+/–) and null (–/–) mice was confirmed by Southern blot hybridization analysis (Figure 1B). Immunoblot analyses confirmed the absence of epimorphin in the small intestine, colon, kidney, liver, and testis of *epimorphin*$^{-/-}$ mice and demonstrated decreased epimorphin in *epimorphin* $^{+/-}$ mice (Figure 1C).

To determine whether the decrease in epimorphin (identical to rat syntaxin 2) expression might affect expression of other syntaxins in the heterozygous and null mice, immunoblots using specific anti–syntaxin 1 and anti–syntaxin 4 antibodies were performed, with protein from intestine, colon, liver, kidney, lung, testis, and brain (for syntaxin 1). Syntaxin 1 was expressed only in brain and was not present in epithelial tissues, including small intestine, colon, and lung from WT, heterozygous, or null mice. Syntaxin 4 was expressed in small intestine, colon, lung, kidney, and testis; syntaxin 4 protein levels were unchanged in *epimorphin*$^{+/+}$, *epimorphin*$^{+/-}$, or *epimorphin*$^{-/-}$ mice (Supplemental Figure 1; supplemental material available online with this article; doi:10.1172/JCI25442DS1).

Male epimorphin$^{-/-}$ *mice are infertile.* Intercrosses of *epimorphin*$^{+/-}$ mice produced the expected ratio of WT (n = 144), heterozygous (n = 250), and homozygous mutant mice (n = 126). Male and female *epimorphin*$^{-/-}$ mice were viable, grew normally to adulthood, and appeared healthy without excess mortality for up to 1 year of observation. Organogenesis was intact. Hair growth and patterning as well as skin quality and integrity appeared intact.

Breeding pairs that included male *epimorphin*$^{-/-}$ mice were unsuccessful at producing offspring whereas matings that included female *epimorphin*$^{+/-}$ or *epimorphin*$^{-/-}$ with male *epimorphin*$^{+/+}$ or *epimorphin*$^{+/-}$ mice were successful (Table 1). The results of these pairings indicate that male *epimorphin*$^{-/-}$ mice are infertile. Compared with heterozygotes, *epimorphin*$^{-/-}$ females gave birth to smaller litters (P < 0.05; Table 1). However, the number of *epimorphin*$^{+/-}$ and *epimorphin*$^{-/-}$ pups followed the expected Mendelian inheritance pattern. *Epimorphin*$^{-/-}$ and *epimorphin*$^{+/-}$ dams nursed their pups without apparent difficulty.

To evaluate infertility in the male epimorphin null mice, testicular development and morphology were analyzed. At 3 weeks postpartum, the testes of *epimorphin*$^{-/-}$ mice weighed 20% less than those of WT mice (Figure 2A). By 4 months, the testes of *epimorphin*$^{-/-}$ mice weighed less than 50% of WT mouse testes (Figure 2A). Histological evaluation demonstrated profound germ cell degeneration in the testes of adult *epimorphin*$^{-/-}$ mice (Figure 2, C and D) compared with WT (Figure 2B). Spermatogonia and spermatocytes were present in seminiferous tubules, but spermatids were depleted and mature spermatozoa were not seen. Meiotic germ cells were

Table 1
Reproductive defects in *epimorphin*$^{-/-}$ mice

Genotype			
Male (n)	Female (n)	Litter number	Litter size (mean ± SEM)
+/+ (1)	–/– (3)	3	6.3 ± 1.2
+/– (4)	–/– (7)	12	6.5 ± 0.8[A]
+/– (20)	+/– (30)	62	8.4 ± 0.2
–/– (10)	+/+ (10)	0	0
	+/– (10)	0	0
	–/– (10)	0	0

Breeding pairs of various genotypes of mice, ranging from 8 to 16 weeks old, were caged together for 10–16 weeks. Each male was housed with 1–4 females. Pregnant females were separated before delivery. The number of pups in each litter was recorded within 24 hours after birth.
[A]P < 0.05 compared with male *epimorphin*$^{+/-}$ × female *epimorphin*$^{+/-}$.

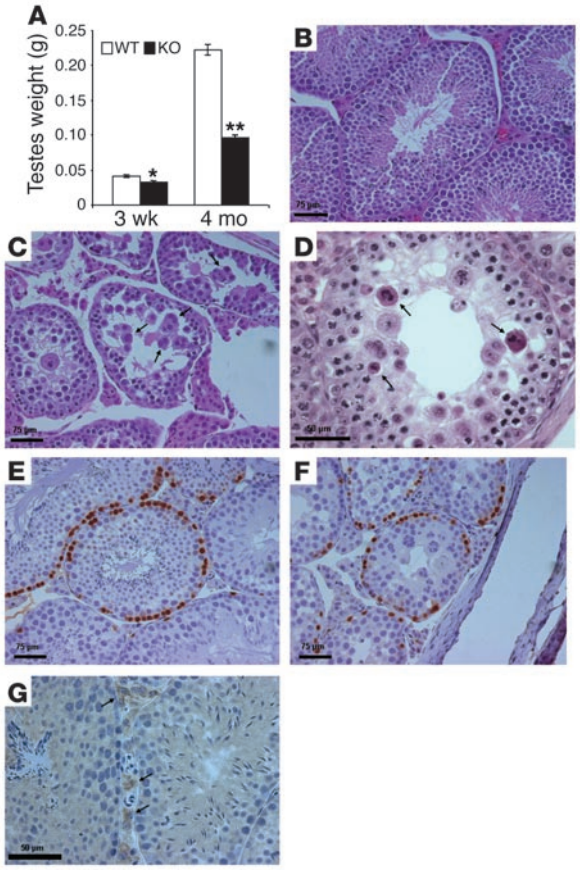

Figure 2
Comparison of testicular weight and histology in WT and *epimorphin*$^{-/-}$ mice. (**A**) Testes of 3-week-old and 4-month-old WT (n = 16 and 29, respectively) and *epimorphin*$^{-/-}$ (KO) mice (n = 16 and 13, respectively) were dissected and weighed. Data are expressed as mean ± SEM. $^{*}P < 0.005$; $^{**}P < 0.001$. (**B**–**G**) Testes from 3-month-old mice of various genotypes. (**B**) Representative H&E-stained cross section of testis from a WT mouse, demonstrating normal spermatogenesis. (**C**) Representative cross section from an *epimorphin*$^{-/-}$ mouse. Note the absence of spermatids in the seminiferous tubules and the detachment of meiotic germ cells in clusters from the basal lamina of seminiferous tubules (arrows). (**D**) Cross section from an *epimorphin*$^{-/-}$ mouse, demonstrating germ cells in the seminiferous tubule exhibiting the darkly stained condensed nuclei that are characteristic of apoptotic cells (arrows). (**E** and **F**) Sections from a WT testis (**E**) and an *epimorphin*$^{-/-}$ testis (**F**) incubated with an anti–5-BrdU antibody to detect proliferating spermatogonia, as described in Methods. (**G**). Immunohistochemical analysis of epimorphin expression in normal testes. Sections were incubated with an anti–syntaxin 2 antibody preabsorbed with testis protein isolated from *epimorphin*$^{-/-}$ mice and were stained as described in Methods. Arrows indicate brown stain in Leydig cells.

detached in clusters from the basal lamina of seminiferous tubules (Figure 2C). Increased numbers of apoptotic germ cells exhibiting darkly stained condensed nuclei were found in many seminiferous tubules (Figure 2D). Proliferation of spermatogonia appeared normal in *epimorphin*$^{-/-}$ mice, as indicated by immunohistochemical detection of 5-BrdU incorporation in WT (Figure 2E) or *epimorphin*$^{-/-}$ mice (Figure 2F), but no mature sperm were produced in *epimorphin*$^{-/-}$ mice. These findings indicate that the formation of mature spermatozoa was compromised in *epimorphin*$^{-/-}$ mice.

Localization of epimorphin expression in the testis was evaluated by immunohistochemical techniques. A polyclonal anti-epimorphin (syntaxin 2) antibody purified by preabsorption with epimorphin null mouse testis protein was utilized. In WT testes, epimorphin was most abundantly expressed in Leydig cells (Figure 2G); much lighter brown staining was also found in cells of the seminiferous tubules. Staining was absent in epimorphin null testes.

Increased intestinal crypt cell proliferation, crypt depths, villus heights, and crypt fission in neonatal, suckling mice. Previous data suggested that epimorphin regulates cellular proliferation and crypt villus morphogenesis in the gut epithelium (15, 16). Our initial phenotypic analysis of the *epimorphin*$^{-/-}$mouse revealed that, in addition to changes in testicular size, small bowel and colonic lengths were increased in 4-month-old *epimorphin*$^{-/-}$ mice compared with WT (Figure 3, A and B). In addition, liver weights were increased in adult *epimorphin*$^{-/-}$mice compared with WT littermates (Figure 3C). No differences in other organ weights were noted in null versus WT mice. These findings suggest that epimorphin deletion affects the growth of intestine and liver in neonatal life, when accelerated organ growth is required for normal development.

Therefore, histological and detailed morphometric analyses were performed to elucidate the effects of epimorphin deletion on the ontogeny and growth of the small intestine. Morphometric analyses using 3- week-old and 4-month-old mice were performed (Figures 4 and 5). Both villus lengths and crypt depths were signifi-

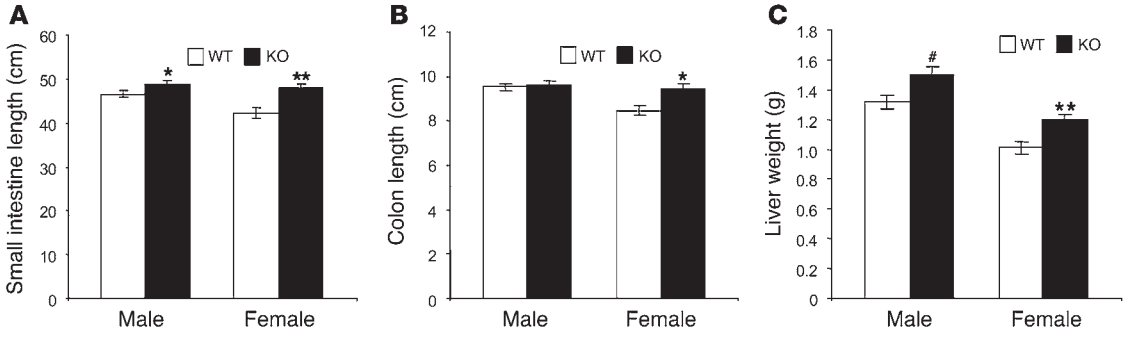

Figure 3
Comparison of small intestinal and colonic lengths and liver weights in adult (4 months old) WT and *epimorphin*$^{-/-}$ mice. (**A**) Small intestinal lengths, (**B**) colonic lengths, and (**C**) liver weights were measured in 4-month-old WT (male, n = 16; female, n = 9) and *epimorphin*$^{-/-}$ (male, n = 13; female, n = 16) mice as described in Methods. Data are expressed as means ± SEM. $^{*}P < 0.05$; $^{**}P < 0.005$; $^{\#}P < 0.02$.

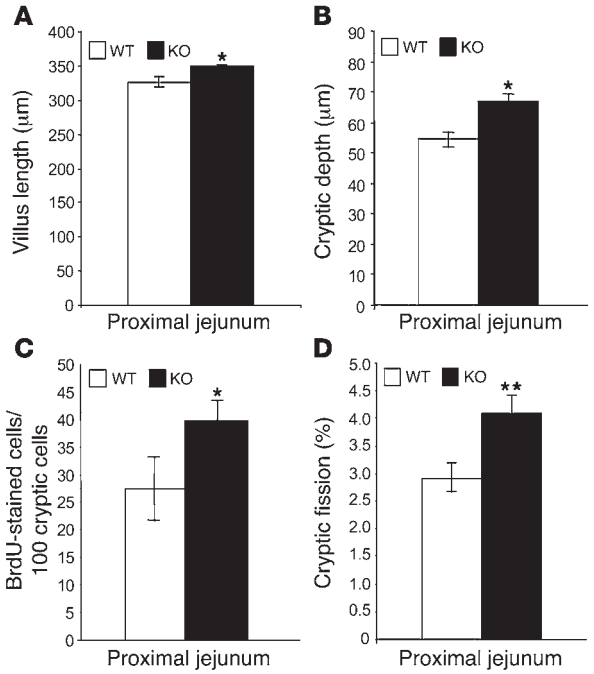

Figure 4
Quantitative morphometric analysis of the small intestines of 3-week-old WT and *epimorphin*$^{-/-}$ mice. (**A**) Villus heights, (**B**) crypt depths, (**C**) crypt cell proliferation, i.e., 5-BrdU incorporation, and (**D**) crypt fission in proximal jejunum from WT and *epimorphin*$^{-/-}$ mice were measured as described in Methods. Data are expressed as mean ± SEM. WT, $n = 14$; KO, $n = 16$. *$P < 0.05$; **$P < 0.02$.

cantly increased in the small intestine of 3-week-old *epimorphin*$^{-/-}$ mice compared with WT littermates (Figure 4, A and B). Crypt cell proliferation was also increased in *epimorphin*$^{-/-}$ mice (Figures 4C and 5, A and B). Villus length, crypt depth, and crypt cell proliferation were also increased in *epimorphin*$^{+/-}$ mice compared with WT mice ($P < 0.001$ for villus length; $P < 0.02$ for crypt depth; and $P < 0.01$ for crypt cell proliferation). In suckling mice, accelerated small bowel growth occurs by crypt fission. The percentage of duplicated small intestinal crypts was greater in 3-week-old *epimorphin*$^{-/-}$ mice compared with WT mice (Figures 4D and 5, B and C). Crypt cell apoptosis was unchanged (data not shown). Crypt and villus morphology appeared generally normal in the small intestine of *epimorphin*$^{-/-}$ mice. The small intestinal crypts of Lieberkühn are the site of the putative epithelial stem cells and are the source of proliferating precursor cells that give rise to the 4 major differentiated epithelial cell types, including enterocytes, goblet cells, enteroendocrine cells, and Paneth cells. All 4 epithelial cell types were present. However, in 3-month-old mice, and even as early as 3 weeks after birth, scattered foci of abnormal villus branching were present in intestine of some *epimorphin*$^{-/-}$ mice (Figure 5D). At 3 weeks of age, there were no significant differences in the lengths of small intestine and colon and in the weights of stomach, heart, lung, liver, spleen, and kidney between *epimorphin*$^{-/-}$ and WT mice (data not shown).

Cell-specific epimorphin expression was studied in WT mouse intestine by immunohistochemical analysis, using an anti–syntaxin 2 antibody that was preabsorbed with null mouse intestinal protein. As previously described (13, 14), epimorphin is expressed in pericryptal stromal cells (Figure 5E).

Epimorphin deletion alters Bmp and Wnt/β-catenin signaling pathways. Elimination of epimorphin resulted in increased crypt cell proliferation and crypt fission in the neonatal gut, suggesting that epimorphin might affect the stem cell niche and particularly the production of proliferating daughter cells in the crypt. We therefore analyzed the expression of Bmps and other members of the TGF-β superfamily in the *epimorphin*$^{-/-}$ and WT gut that are known to affect the stem cell niche and the production of proliferating daughter cells. Our previous data (15) indicated that Bmp 4 mRNA expression was increased in epimorphin-transfected (overexpressing) gut myofibroblasts, suggesting that regulation of Bmps might play a role in epimorphin's effects on cocultured epithelial cells. Bmp signaling has an antiproliferative effect in normal gut and may act on the crypt epithelium via the Wnt pathway by inhibiting nuclear accumulation of β-catenin (19). To determine whether enhanced proliferation in *epimorphin*$^{-/-}$ mice was associated with decreased Bmp expression, quantitative RT-PCR was performed using total RNA prepared from full thickness proximal jejunum of null and WT mice. Bmp4 mRNA levels were decreased in null versus WT gut (22% decrease, $P = 0.03$; Table 2). Bmp2 mRNA levels

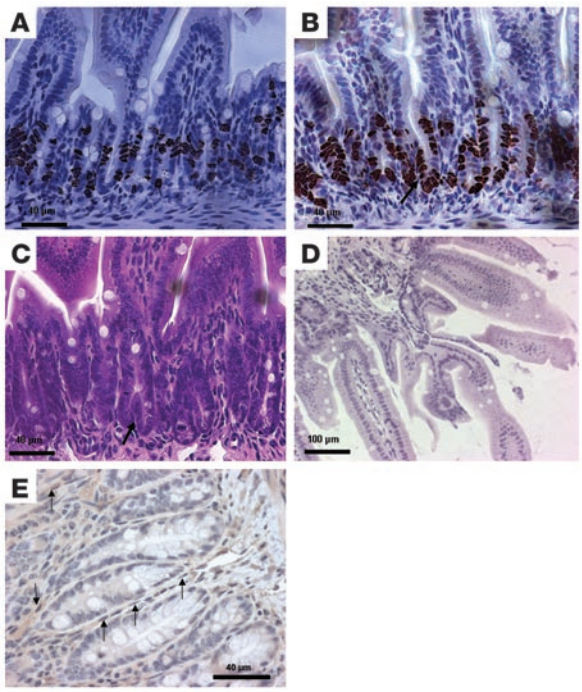

Figure 5
Crypt cell proliferation, crypt fission, villus morphology, and epimorphin expression in small intestine of *epimorphin*$^{-/-}$ mice. (**A** and **B**) Representative histologic section depicting immunohistochemical detection of 5-BrdU incorporation into crypt epithelial cells in proximal jejunum of 3-week-old WT (**A**) and *epimorphin*$^{-/-}$ (**B**) mice. Note the increase in 5-BrdU–labeled cells in the null mice. (**B** and **C**) Crypt fission is detected in proximal jejunum of *epimorphin*$^{-/-}$ mice in 5-BrdU–immunostained tissue (**B**, arrow) or in H&E-stained tissue (**C**, arrow). (**D**) Abnormal villus morphology in 3-week-old *epimorphin*$^{-/-}$ intestine. (**E**) Epimorphin expression in stromal cells of jejunum. Epimorphin was detected with an anti–epimorphin–syntaxin 2 antibody, which was preabsorbed with purified intestinal protein from *epimorphin*$^{-/-}$ mouse jejunum, as described in Methods. Arrows depict stromal myofibroblasts that express epimorphin.

Table 2
Intestinal expression of Wnt and Bmp target genes and TGF-β family genes in null versus WT mice

Gene	Fold change *epimorphin*$^{-/-}$/WT	*P* value
Bmp4[A]	0.78	0.03
Bmp2[A]	0.83	0.08
TGF-β1[A]	0.89	0.4
TGF-β2[A]	0.95	0.5
TGF-β3[A]	1.04	0.9
c-Myc[B]	1.29	0.04
Cyclin D1[B]	1.26	0.04
Smad7[B]	0.83	0.01

Quantitative real-time RT-PCR analyses were performed on proximal jejunal total RNA isolated as described in Methods. Results are expressed as fold change in steady state mRNA levels: *epimorphin*$^{-/-}$/WT. [A]WT, $n = 10$; *epimorphin*$^{-/-}$, $n = 13$; [B]WT, $n = 18$; *epimorphin*$^{-/-}$, $n = 20$.

also tended to be decreased; (17% decrease, $P = 0.08$). In addition, the expression of the Bmp downstream effector molecule Smad7 was significantly decreased (17% decrease, $P = 0.01$). Smad7 is also a downstream target of TGF-β signaling; thus the expression of TGF-β1, -β2, and -β3 was examined by quantitative RT-PCR and was unchanged in null compared with WT mice. The effect on Bmp signaling therefore appears to be specific in *epimorphin*$^{-/-}$ mouse gut. To determine whether Wnt/β-catenin signaling is also regulated, the expression of 2 downstream targets of Wnt, c-myc and cyclin D1, was quantified; a 26% increase in cyclin D1 expression and a 29% increase in c-myc expression were found in null compared with WT mouse gut ($P = 0.04$).

To further implicate increased β-catenin signaling as a mechanism for increased c-myc and cyclin D1 expression and increased BrdU incorporation in *epimorphin*$^{-/-}$ intestine, nuclear fractions were prepared from the intestines of WT and null mice. Immunoblot analysis was performed to assess nuclear and cytoplasmic/membrane β-catenin levels. An increase in nuclear β-catenin accumulation was noted in *epimorphin*$^{-/-}$ mice compared with heterozygous and WT mice (Figure 6, A and B). To further explore these results, immunohistochemical analysis was performed to detect β-catenin staining (Supplemental Figure 2). An increase in intensity of staining in the nuclei of the crypt was noted in the *epimorphin*$^{-/-}$ mice, consistent with the immunoblot results. In addition, membrane staining was increased throughout the crypt and along the villus.

To provide further evidence that Bmp signaling is regulated by epimorphin and to determine the cell-specific expression of the Bmps in relation to epimorphin, we examined Bmp expression in cocultures of intestinal epithelial Caco-2 cells and intestinal myofibroblasts that overexpress epimorphin or in which epimorphin expression is inhibited (as per ref. 15). The well-characterized Mic216 ileal intestinal myofibroblast cell line (14, 15) was transfected with the full-length epimorphin cDNA in sense or antisense orientations, as previously described (15). Epimorphin was overexpressed by 3- to 4-fold or was inhibited compared with vector control cells, as determined by immunoblot (data not shown). These myofibroblasts were then cocultured with Caco-2 cells, injected into the subcutaneous space of nude mice, and grown for 6 weeks (Figure 7). In myofibroblast–Caco-2 cell grafts that overexpress epimorphin, abundant Bmp expression was detected by immunohistochemical techniques (Figure 7A) using an antibody specific for Bmp2 and Bmp4. Bmp expression was found in both myofibroblasts and Caco-2 cells. In contrast, in cocultures in which epimorphin expression was suppressed, Bmp expression was inhibited in epithelial and myofibroblast cells (Figure 7B).

As we previously reported (15), Caco-2 cells, when cocultured with myofibroblasts in which epimorphin expression is inhibited (by stable transfection with epimorphin antisense cDNA), grow rapidly over the surface of the myofibroblasts, producing large Caco-2 cell colonies (Figure 8, A and B). In contrast, Caco-2 cells cocultured with epimorphin-overexpressing myofibroblasts form small, round, discrete colonies (15). To further test our hypothesis that the effect of epimorphin on intestinal growth is at least in part mediated by Bmps, we treated Caco-2–antisense epimorphin myofibroblast cocultures with Bmp4 (100–200 ng/ml) and observed whether or not addition of Bmps could inhibit Caco-2 cell colony growth on antisense myofibroblasts. As indicated in Figure 8, C and D, addition of Bmp4 resulted in the formation of round, discrete Caco-2 cell colonies (compared with control panels in Figure 8, A and B), reversing the effects of epimorphin inhibition. The appearance of these colonies reproduces what was previously reported for Caco-2 cells cocultured on epimorphin-overexpressing myofibroblasts (ref. 15 and data not shown).

Protection from dextran sodium sulfate–induced colon epithelial injury in epimorphin null mice. The gut trophic effects of epimorphin deletion in neonatal mice indicated by an increase in crypt cell proliferation suggested that downregulating epimorphin expression could also enhance repair responses following intestinal injury. To test this hypothesis, a well-characterized colitis model was used to study mucosal injury and repair responses. Dextran sodium sulfate (DSS) induces a chemical colitis characterized by mucosal ulceration, epithelial barrier disruption, and gland destruction followed by crypt cell proliferation and mucosal repair (20, 21). The induction and severity of DSS-induced colitis was compared in WT and *epimorphin*$^{-/-}$ mice.

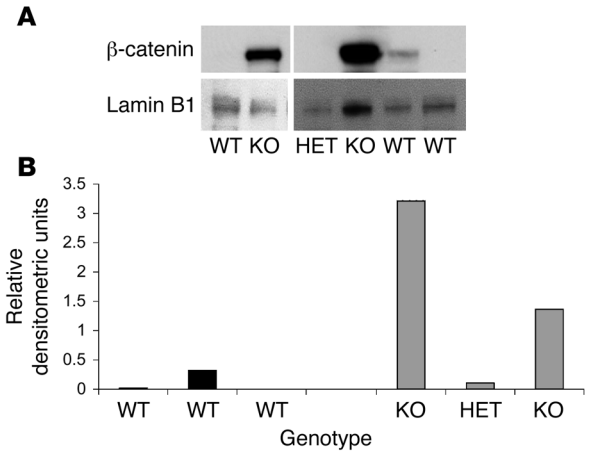

Figure 6
β-catenin expression in *epimorphin*$^{-/-}$ and WT mouse intestine. Nuclear protein isolation was performed as described in Methods. (**A**) Representative immunoblots of intestinal nuclear protein from WT, *epimorphin*$^{-/-}$, and *epimorphin*$^{+/-}$ (HET) mice. Nuclear proteins (20 μg per lane) were electrophoresed, and immunoblots were incubated with an anti–β-catenin antibody. Blots were sequentially probed with an anti-lamin B1 antibody to control for differences in loading. (**B**) Quantification of nuclear β-catenin expression normalized to lamin B1 expression.

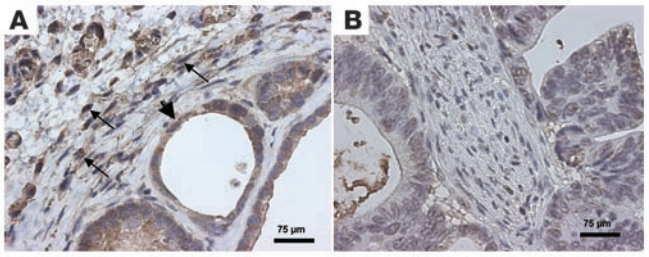

Figure 7
Immunohistochemical analysis of Bmp expression in epimorphin-transfected myofibroblast–Caco-2 cell grafts in nude mice. Bmp expression was detected with an anti-Bmp2/Bmp4 antibody as described in Methods. (**A**) Bmp expression in grafts containing epimorphin-overexpressing myofibroblasts. Thin arrows indicate stromal myofibroblasts that exhibit increased Bmp expression. Thick arrow indicates Caco-2 epithelial cells that also show Bmp expression. (**B**) Bmp expression in grafts containing myofibroblasts in which epimorphin is inhibited. There is a marked decrease in Bmp expression in stromal myofibroblasts and epithelial Caco-2 cells compared with **A**.

Cohorts of WT and *epimorphin*$^{-/-}$ mice were provided with either water or water containing 5% (w/v) DSS for 7 days. Body weight change, stool consistency, and the presence of fecal occult or gross blood were recorded daily and used to calculate a clinical score (see Methods) that reflected overall disease severity. After 7 days of DSS administration, body weight loss was less severe in *epimorphin*$^{-/-}$ mice than in WT mice (–11.3% versus –17.6%, Table 3). Detection of fecal occult blood was also delayed in *epimorphin*$^{-/-}$ mice and the morbidity, as measured by the clinical scores, was less in the null mice (Table 3). The severity of mucosal injury assessed microscopically correlated with the clinical score. Thus, histologic damage to the colonic mucosal glandular architecture was not as severe or extensive in *epimorphin*$^{-/-}$ mice (Figures 9 and 10, A and B). *Epimorphin*$^{-/-}$ mice had a lower crypt damage score in the proximal colon (Figure 9A) as determined by the criteria in ref. 22. There were also significantly more areas of grade II mucosal injury and fewer areas of grade IV (23, 24) mucosal injury (Figures 9B and 10, A and B). These differences were more apparent in the proximal colon. After DSS treatment, crypt cell proliferation rates in the colonic mucosa of *epimorphin*$^{-/-}$ mice were further increased compared with WT mice in areas adjacent to ulcerations (as described in ref. 21) as well as distant from them (Figures 9C and 10, C and D). In proximal colon, 20.9% and 7.2% BrdU-stained crypt epithelial cells were detected in *epimorphin*$^{-/-}$ and WT mice, respectively (Figures 9C and 10, C and D). In distal colon, 24.2% crypt epithelial cells were BrdU stained in *epimorphin*$^{-/-}$ mice while only 3.4% crypt epithelial cells were BrdU-stained in WT mice. In addition, *epimorphin*$^{-/-}$ mice demonstrated enhanced crypt cell hyperplasia in nonulcerated areas following DSS injury. There were more epithelial cells per crypt in the *epimorphin*$^{-/-}$ mice compared with WT mice in both proximal and distal colons of DSS-treated mice (Figure 9D), consistent with increased proliferation in *epimorphin*$^{-/-}$ mice. These findings suggest that the reduced severity of colitis in *epimorphin*$^{-/-}$ mice was probably due to mucosal protective effects resulting from the increase in intestinal epithelial proliferation.

Discussion

Epimorphin$^{-/-}$ mice were generated to study the in vivo role of this mesenchymal protein on gut morphogenesis. *Epimorphin*$^{-/-}$ mice exhibited increased intestinal growth, with increased crypt cell proliferation and crypt fission resulting in lengthening of the small bowel. We hypothesized that the increased proliferative capacity of the *epimorphin*$^{-/-}$ intestine might provide protection from mucosal injury induced by DSS due to enhanced epithelial regeneration. Null mice lost less weight, had delayed onset of gastrointestinal bleeding detected by fecal occult blood testing, and sustained less severe histologic injury, resulting in lower clinical activity scores. Our studies suggest a unique role for stromal epimorphin in regulating epithelial cell proliferation in normal and regenerating gut.

In addition to the intestinal phenotype, *epimorphin*$^{-/-}$ mice had increased liver weights, and male mice were infertile due to profound abnormalities in spermatogenesis. Thus, although epimorphin is expressed in many additional epithelial tissues (e.g., mammary gland, kidney, and lung), the phenotypic changes were readily apparent only in intestine, liver, and testis. This suggests that, compared with other organs, epimorphin plays a more critical role in the regulation of gastrointestinal epithelial proliferation and testicular spermatogenesis. The gastrointestinal tract and liver epithelium are both subject to direct or indirect exposure to, and in some cases injury from, luminal and ingested substances (e.g., food, toxins, and bacteria). In addition, both the liver and the small intestine have significant regenerative capability after loss of functional mass due to insults, such as ischemic injury. The generation of congenic *epimorphin*$^{-/-}$ mice may shed more light on epimorphin's role in other organs.

The small intestinal epithelium has a high basal rate of proliferation. Epithelial stem cells located near the base of the crypts of Lieberkühn give rise to proliferating transit cells that differentiate into the 4 primary epithelial cell types as they migrate from crypt to villus tip. Complete renewal of the mucosal absorptive surface area occurs approximately every 3–5 days in the rodent and human. Tight regulation of this process is critical for maintaining

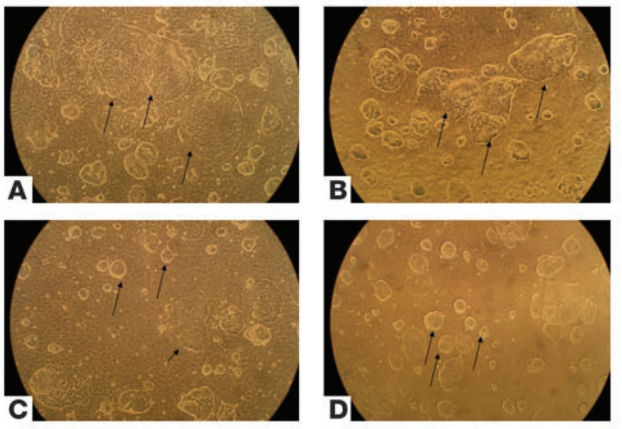

Figure 8
Bmp4 alters growth and spreading of Caco-2 cells cocultured with epimorphin antisense-transfected myofibroblasts. (**A** and **B**) Caco-2 cells were cocultured with epimorphin antisense-transfected myofibroblasts, in which epimorphin expression had been inhibited, in vehicle control media. Large Caco-2 cell colonies are noted, spreading over the myofibroblast surface (thin arrows). A few scattered smaller colonies are also seen. Two different antisense transfected myofibroblast cell clones are depicted in **A** and **B**. (**C** and **D**) Addition of 100 ng/ml (**C**) or 200 ng/ml (**D**) Bmp4 to epimorphin-antisense–transfected myofibroblast–Caco-2 cocultures. Thin arrows depict Caco-2 colonies. Note the appearance of multiple small round colonies resulting from addition of Bmp4. Only a few scattered larger Caco-2 cell colonies are seen, in **C** only (short arrow). Magnification, ×100.

Table 3
Reduced severity of DSS-induced colitis in *epimorphin*$^{-/-}$ mice

	Body weight loss (%)	Day FOB first detected	Clinical score
+/+ Vehicle	2.4 ± 1.3	N/A	0.8 ± 0.3
–/– Vehicle	2.1 ± 1.5	N/A	1.0 ± 0.3
+/+ DSS	17.6 ± 1.7	2.9 ± 0.3	3.3 ± 0.2
–/– DSS	11.3 ± 1.8^{A}	4.1 ± 0.2^{B}	2.6 ± 0.2^{A}

Male WT (+/+) or *epimorphin*$^{-/-}$ mice received drinking water (vehicle) with or without 5% DSS. Body weight change, stool consistency, and detection of intestinal bleeding were recorded daily, and a clinical score (scale 0–4) was calculated as described in Methods. Changes in body weight after DSS administration for 7 days were expressed as percentage changes from initial weight. WT and *epimorphin*$^{-/-}$ mice receiving water only, $n = 6$ and 6, respectively; WT and *epimorphin*$^{-/-}$ mice receiving 5% DSS in drinking water, $n = 14$ and 11, respectively. Data are expressed as means ± SEM. $^{A}P < 0.02$ and $^{B}P < 0.005$ versus WT DSS. FOB, fecal occult blood.

the intestinal mucosa and for preventing tumorigenesis. Our data suggest that epimorphin normally functions as a negative regulator of epithelial proliferation; therefore it is not surprising that the effects of epimorphin deletion were more easily detectable in the highly proliferative intestine.

Intestinal subepithelial myofibroblasts (ISEMFs) are the source of epimorphin in the mature small bowel (13, 15) and colon (25). These cells form a pericryptal network that also extends into the villus core. ISEMFs are characterized by their location, expression of smooth muscle α-actin, and absence of desmin (14, 26, 27). ISEMFs are a source of paracrine growth factors supporting the proliferation and differentiation of epithelium (26). Functional heterogeneity has been demonstrated in this population (14). ISEMFs express several Bmps, which act on the epithelium to inhibit crypt cell proliferation and crypt fission (15, 19) and have also been postulated to produce Wnt signaling factors (6, 28). Epimorphin's homology to the syntaxins (12, 29) suggests that it may play a novel role in regulating the secretion of a subset of myofibroblast-derived soluble factors that "condition" the crypt, such as the Bmps. Epimorphin deletion resulted in a significant decrease in Bmp and Smad7 expression and an increase in expression of β-catenin and of several downstream targets of the Wnt/β-catenin signaling pathway, including c-myc and cyclin D1. Our data provide further support for the findings of He et al. (19) showing that decreased Bmp expression can affect intestinal stem cells, resulting in increased crypt cell proliferation and crypt fission. Bmps appear to inhibit nuclear accumulation of β-catenin by enhancing phosphatase and tensin homolog (PTEN) activity, which represses Akt activity that is required, with Wnts, to fully activate β-catenin in stem cells and induce proliferation (19). A decrease in local Bmp production and/or secretion induced by epimorphin deletion would be expected to act on stem/progenitor cells to increase crypt cell proliferation and crypt fission. Further support for this mechanism comes from our prior studies showing that myofibroblasts overexpressing epimorphin induced the formation of small, compact colonies of cocultured epithelial cells (15) and had increased Bmp4 expres-

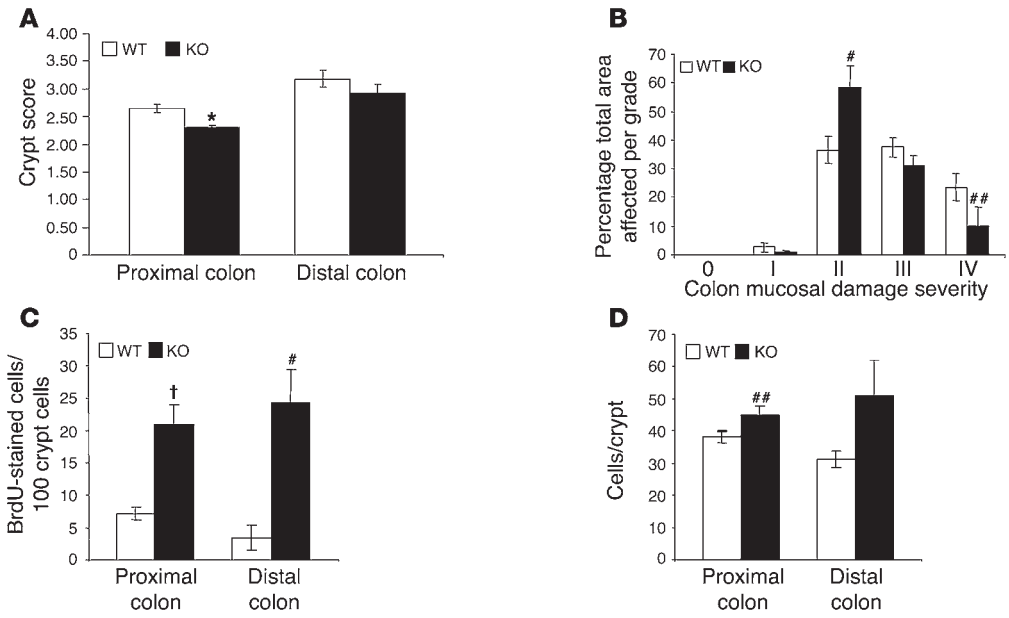

Figure 9
Comparison of colonic epithelial injury and proliferation after DSS administration in WT and *epimorphin*$^{-/-}$ mice. Male WT and *epimorphin*$^{-/-}$ mice were sacrificed after receiving drinking water with or without 5% DSS for 7 days. The colons were collected and processed for histological studies as described in Methods. (**A**) The severity of epithelial injury was assessed by a grading system (22) described in Methods. Proximal colon, WT and KO, $n = 12$ and 9, respectively; $^{*}P < 0.01$; distal colon, WT and KO, $n = 11$ and 11, respectively. Data are expressed as means ± SEM. (**B**). The percentages of fields involved with either grade I, II, III, or IV injury (23, 24) were quantified as described in Methods. WT, $n = 9$; KO, $n = 9$. Data are expressed as means ± SEM. $^{\#}P < 0.005$, $^{\#\#}P < 0.05$. (**C**) Colonic crypt cell proliferation was assessed by quantification of 5-BrdU incorporation. Proximal colon, WT and KO, $n = 12$ and 7, respectively; distal colon, WT and KO, $n = 6$ and 4, respectively. Data are expressed as means ± SEM. $^{\dagger}P < 0.001$. (**D**) Number of epithelial cells per colonic crypt. Proximal colon, WT and KO, $n = 12$ and 7, respectively; distal colon, WT and KO, $n = 6$ and 4, respectively. Data are expressed as means ± SEM. Increased crypt cell proliferation and crypt cell hyperplasia are noted in KO mice.

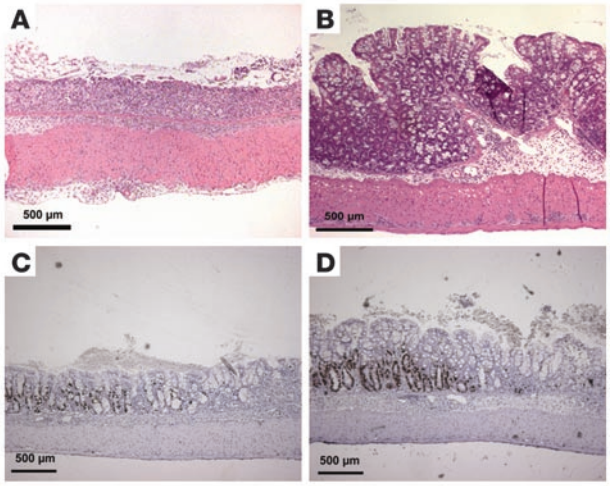

Figure 10
Representative histologic sections demonstrating more severe mucosal injury in DSS-treated WT mouse colon and enhanced crypt cell proliferation in DSS-treated *epimorphin*$^{-/-}$ mouse colon. (**A** and **B**) Inflammatory cell infiltration and epithelial erosions were evident in the colonic mucosa after 7 days of DSS administration. However, as shown in representative H&E-stained histologic sections, ulcerative lesions were more common in WT mice (**A**) and less severe injury (**B**) was more frequent in *epimorphin*$^{-/-}$ mice. (**C** and **D**) Crypt cell proliferation in colonic mucosa adjacent to ulcerative lesions in DSS-treated WT (**C**) and *epimorphin*$^{-/-}$ mice (**D**).

sion. Conversely, myofibroblasts in which epimorphin expression was inhibited stimulated spreading and proliferation of cocultured epithelium (15). In the present study, we have shown that addition of Bmp4 reversed this effect (Figure 8). The suppressive effect of Bmp signaling on intestinal crypt formation and polyp growth has also been demonstrated in transgenic mice that overexpress noggin, a Bmp inhibitor, in the gut; these mice formed numerous ectopic crypt units throughout the gut (5). Our data suggest that Bmp expression is decreased in both myofibroblast and epithelial cells (Figure 7). We have previously shown that epimorphin is expressed in myofibroblasts but not in Caco-2 or other epithelial cells (15, 16); thus the effects of epimorphin deletion on Bmp expression in epithelial cells are not likely to be direct but rather related to myofibroblast-epithelial interactions mediated by epimorphin.

Increased crypt fission in the intestine of juvenile *epimorphin*$^{-/-}$ mice indicates that epimorphin regulates not only epithelial proliferation but also crypt duplication in the intestine. Crypt fission is characterized by the presence of a bisecting fissure at the base of the parental crypt and the longitudinal ascendance of the fissure, leading to the production of 2 daughter crypts. Crypt duplication by fission occurs with increased frequency during a brief period of postnatal life, from approximately 5 to 21 days after birth (30). Bmps are also involved in the regulation of de novo crypt formation in the intestine (5). Thus, the increased crypt fission seen in epimorphin null mice may also be mediated via effects on Bmp signaling. Noggin-expressing transgenic mice, which exhibit complete inhibition of Bmp signaling, form polyps in the small bowel (5); we observed abnormal villus morphology with branching villi in *epimorphin*$^{-/-}$ mice (Figure 4D).

Overexpression of a soluble form of epimorphin in mammary gland (using the whey acidic protein promoter to overexpress full-length epimorphin fused to the NH2-terminal signal sequence of IL-2) promotes tumorigenesis in aged mice (31). The fact that this phenotype results from overexpression of epimorphin (which has been shown to promote mammary morphogenesis but does not directly stimulate proliferation; ref. 7) and thus is opposite the observed phenotype in the *epimorphin*$^{-/-}$ mouse intestine suggests disparate roles for epimorphin in different tissues and possibly unique effects of the soluble form of epimorphin.

Epimorphin$^{-/-}$ mice were partially protected from colitis induced by DSS. DSS colitis is thought to result from disruption of the normal epithelial barrier, since changes in permeability occur before the onset of frank inflammation (20, 32). This concept is also supported by studies in intestinal trefoil factor null mice. Absence of this protein, which is important in epithelial repair, results in markedly worse colitis compared with WT mice (20, 33). Also, transgenic mice in which a dominant-negative TGF-β is overexpressed in intestine (34) have worsened colitis and delayed healing. In our mice, protection occurred early in the course of the colitis (e.g., fecal occult blood appearance was delayed from an average of 2.9 days following the start of DSS treatment in WT mice to 4 days after the beginning of treatment in null mice), suggesting that enhanced crypt cell proliferation allowed for rapid restoration of the mucosal surface barrier, increasing resistance to ulceration and subsequent inflammatory response.

A remarkable increase in colonic crypt cell proliferation was seen in the DSS-treated *epimorphin*$^{-/-}$ colon compared with the WT colon. Previous studies in the DSS colitis model showed that intact colonic mucosa adjacent to ulcerations exhibited enhanced crypt cell proliferation compared with crypts in uninvolved mucosa (21). We found that the *epimorphin*$^{-/-}$ DSS colon showed a marked augmentation of crypt cell proliferation in mucosa adjacent to the ulcerations as well as in the intact mucosa in other areas of the DSS-treated colon compared with WT DSS-treated colon. Thus, in DSS-induced colitis, deletion of epimorphin may further enhance proliferation, as we postulated to occur in the normal gut.

Alternatively, in the colitis model, other mediators may be responsible for the protective effects resulting from epimorphin deficiency. Intestinal myofibroblasts can react to inflammatory signals by expressing cytokines (26, 35–37). For example, exposure to bacteria activates these cells (38). Myofibroblasts express toll-like receptors 1–9, NOD1, NOD2, and Myd88, and lipopolysaccharide upregulates a subset of toll-like receptors in these cells (37) that in turn leads to release of mediators of inflammation. In DSS colitis, loss of barrier function is thought to permit entrance of bacteria into the subepithelial space, thereby eliciting an inflammatory response (20). Loss of epimorphin did not appear to affect the myofibroblast response by decreasing secretion of cytokines or other proinflammatory molecules and thus reducing the inflammatory response since cytokine expression was unchanged in *epimorphin*$^{-/-}$ mice. Finally, it is possible, albeit less likely, that macrophage function is affected in *epimorphin*$^{-/-}$ mice. Syntaxin 2, the rat homolog of epimorphin, was shown to be expressed in the macrophage although the antibody used in those experiments cross-reacts with syntaxin 4 and 6, which are also expressed in macrophages (39). The latter syntaxins, but not syntaxin 2, have been linked to the regulation of secretion of cytokines such as TNF-α (40, 41), and syntaxin 4 is regulated by LPS (40). Furthermore, our previous studies and those of other investigators show that in the adult gut, epimorphin is expressed in myofibroblasts but not macrophages (13, 25). Thus,

it is likely that elimination of epimorphin expression in intestinal myofibroblasts and not macrophages is the most plausible explanation for the protective effects seen in the DSS colitis model. Further studies will be required to determine the precise mechanism underlying the protection of epimorphin null mice from colitis.

The proliferative phenotype demonstrated in the intestinal epithelium in normal neonatal and in DSS-treated mice is consistent with our previous, albeit indirect in vivo studies of epimorphin function in the gut. For example, epimorphin expression was reduced in the remnant gut following partial small bowel resection (13). In this model of intestinal adaptation, crypt cell proliferation is markedly upregulated. The decrease in epimorphin expression coincided with the onset of enhanced crypt cell proliferation, suggesting that diminished epimorphin expression occurs in concert with increased epithelial proliferation.

The loss of epimorphin also adversely affected germ cell development, as testicular size and spermatogenesis were markedly diminished in the epimorphin null mouse. Disrupted germ cell differentiation and augmented apoptosis were associated with marked depletion of spermatids in the testes of *epimorphin*$^{-/-}$ mice. Seminiferous tubules contained proliferating spermatogonia and spermatocytes, but spermatids and mature spermatozoa were not observed. Sertoli and Leydig cells were present. Our immunohistochemical studies suggest that epimorphin is expressed in Leydig cells (Figure 2), with lower expression in other cells of the seminiferous tubules. Syntaxin 2 is associated with spermatic membranes and is expressed in the acrosomal region of the sperm (42, 43). Thus, a role for syntaxin 2 in the acrosomal reaction had been suggested (42). However, since mature sperm were not produced in *epimorphin*$^{-/-}$ testes, our results indicate that epimorphin plays an earlier role, possibly in the development of spermatids from spermatocytes. Leydig cells were histologically normal in epimorphin null testes, but their function has not been explored in these studies. It is possible that epimorphin deficiency affects the ability of fibroblast-like progenitors of Leydig cells to secrete growth factors, since large quantities of these are produced by these cells from postnatal day 14 to 21 (44). Testicular development was also impaired prior to the time when Leydig cells normally produce and secrete large amounts of testosterone.

Reproductive-related functions were also examined in female epimorphin null mice. The number of pups per litter was reduced in matings of female *epimorphin*$^{-/-}$ mice with male *epimorphin*$^{+/-}$ mice compared with *epimorphin*$^{+/-}$ female mice with male *epimorphin*$^{+/-}$ mice. Since epimorphin is expressed in the inner cell mass and in trophoectoderm, it has been postulated to play a role in trophoblast outgrowth (45). Nevertheless, the ratio of heterozygous to null mice was as expected. Thus, the reduction in litter size was not due to preferential loss of epimorphin null offspring. These observations suggest that a maternal factor might be responsible for the reduction in litter size. Epimorphin has a well-characterized role in mammary gland ductule formation and tubulogenesis (7, 10, 12), yet female epimorphin null mice were able to nurse their pups without difficulty. Thus, mammary gland development was grossly unaffected by epimorphin deficiency. Other maternal factors such as mild placental insufficiency cannot be ruled out at this time and will be further explored in future studies.

In conclusion, the phenotype of *epimorphin*$^{-/-}$ mice suggests several novel in vivo functions for epimorphin. These studies provide evidence that epimorphin is a key regulator of epithelial growth in the intestine and is required for normal testicular morphogenesis and spermatogenesis. The observation that epimorphin deficiency resulted in increased crypt cell proliferation and partial protection from DSS colitis suggests the possibility that modulation of epimorphin expression could be used therapeutically to increase mucosal regeneration following injury to the gut resulting from inflammatory bowel disease or ischemia or following intestinal resection.

Methods

Generation of epimorphin$^{-/-}$ *mice*. A genomic bacterial artificial chromosome (BAC) clone was obtained by screening a 129/SvJ BAC mouse ES cell library with a 350 bp mouse epimorphin cDNA clone (Incyte). Fragments from EcoR I digestion of the BAC clone were subcloned into pBluescript SK(–) (Stratagene). Clones containing the epimorphin gene were identified by colony hybridization and mapped by partial sequencing. To create the 5′ arm, a 4.7 kb fragment upstream of the *epimorphin* initiator ATG was obtained by Bgl I digestion of the BAC clone. To create a GFP knockin construct, pEGFP-N1 (BD Biosciences — Clontech) was used as a template for the amplification of the coding sequence and polyadenylation signal of GFP. A GFP 5′ primer was designed for the introduction of a Bgl I restriction site and the replacement of the *epimorphin* initiator ATG with that of GFP (5′-CGGGCCCGGCCCTGCTGGCCGGTGGGGATGGTGAGCAAGGGCGAG-3′). A GFP 3′ primer was designed to introduce an Apa I site at the 3′ end of the PCR products (5′-GGTTATCCGGCTTTAGCCGTCCCGGGGAATATTTAGTTTTCTTAT-3′). Ligation of the 4.7 kb epimorphin 5′ arm fragment and the Bgl I digested GFP PCR product created an "Epi 5′ arm–GFP" fragment. This fragment was then digested with Apa I and subcloned into the Apa I site of phosphorylated Neo (p-Neo) plasmid 1339 (GenBank accession number AF335420, Embryonic Stem Cell Core, Washington University School of Medicine). The 3.2 kb epimorphin 3′ arm was obtained by Kpn I digestion of the BAC clone and subsequently subcloned into Kpn I site of p-Neo plasmid 1339 containing the Epi 5′ arm-GFP fragment. The construct was sequenced (Protein and Nucleic Acid Chemistry Laboratory, Washington University School of Medicine) at all ligation junctions to ensure base sequence fidelity. The vector was then linearized with BspH I and electroporated into the RW-4 subclone of ES cells derived from 129/SvJ mice (Embryonic Stem Cell Core, Washington University School of Medicine). Genomic DNA was isolated from G418-resistant ES cell colonies. Southern hybridization assays were performed on Hind III digested DNA using a ^{32}P-labeled 150 nucleotide probe corresponding to sequence upstream of the 5′ arm (Figure 1). In 2 out of 120 clones, an expected 10.4 kb band was detected in addition to the 8.7 kb WT band, indicating the replacement of one of the epimorphin alleles by homologous recombination. Complete integration of the targeting construct was confirmed by additional Southern hybridization analysis.

The positive ES clones were individually injected into C57BL/6 blastocysts and implanted into pseudopregnant females. Chimeric founders derived from both lines produced offspring containing the targeted allele when crossed with C57BL/6J females. Intercrosses of the heterozygotes produced viable homozygous *epimorphin*$^{-/-}$ mice at the expected Mendelian frequency in both sexes. The 2 lines of mice were maintained separately on a C57BL/6J 129/SvJ background. *Epimorphin*$^{-/-}$ mice from both lines were phenotypically identical. All experiments were performed within the same generation, using WT littermates of the *epimorphin*$^{-/-}$ mice for controls.

All mice were housed in the Washington University School of Medicine barrier facility in a 12-hour light-dark cycle with free access to food and water. The mice were fed a standard rodent chow diet (PicoLab 20; Purina). Age-matched null mice and their WT littermates were used in all experiments as described in Results. All animal experimentation was approved by the Animal Studies Committee of Washington University School of Medicine.

To evaluate the phenotype of the *epimorphin*$^{-/-}$ mice, mice were weighed and sacrificed at various ages as described. Small intestines and colons were harvested, and their lengths were measured by suspension with a fixed weight (2.6 g). Small intestines were then divided into 4 segments. The proximal 5 cm of the small intestine was collected as duodenum. The remainder was divided into 3 equal parts representing proximal jejunum, distal jejunum, and ileum. Colons were divided into 2 equal parts called proximal colon and distal colon. Testis, liver, spleen, heart, lung, kidney, and stomach were harvested and weighed. Skin was collected for histological analyses. Tissues were frozen in Tissue-Tek O.C.T. Compound (Sakura Finetek) for frozen histologic sections or in liquid nitrogen for total RNA and protein isolation or placed in 10% formalin (Sigma-Aldrich) for histochemical and immunohistochemical analyses.

Microscopic analysis of testicular morphology. Histologic sections were prepared from formalin-fixed, paraffin-embedded, or frozen testes by the Morphology Core of the Washington University Digestive Diseases Research Core Center. Routine H&E staining was performed on paraffin sections. Proliferating cells (spermatogonia) were identified by immunohistochemical detection of the incorporation of 5-bromodeoxyuridine into DNA (see *Analysis of intestinal morphometrics, proliferation, and apoptosis*, below).

Immunohistochemical analyses. Epimorphin expression in WT testis and intestine was analyzed using a polyclonal rabbit anti–syntaxin 2 antibody (1:500 dilution; Synaptic Systems) that was purified by preabsorption with purified protein from epimorphin null mouse testis or intestine (1 μg of antibody incubated with 50 μg protein). Sections were pretreated with Nuclear DECLOAKER reagent (BIOCARE). Antigen-antibody complexes were detected with biotinylated goat anti-rabbit IgG and streptavidin–horseradish peroxidase with tyramide amplification, developed in diaminobenzidine.

Immunohistochemical analyses of BMP expression were performed using a polyclonal goat anti-recombinant human BMP2/4 antibody (1:300 dilution; R&D Systems) that cross-reacts with mouse. Antigen retrieval was performed with citraconic anhydride; antigen-antibody complexes were detected with a biotinylated donkey anti-goat IgG, detected with streptavidin–horseradish peroxidase and diaminobenzidine. Nuclear β-catenin immunostaining was performed using a polyclonal rabbit anti–β-catenin antibody (Sigma-Aldrich, 1:30). Sections were pretreated with Nuclear DECLOAKER reagent (BIOCARE).

Induction and assessment of DSS-induced colitis. The well-established model of DSS-induced colitis was utilized (20, 23, 34). Male WT and *epimorphin*$^{-/-}$ mice of 12 to 18 weeks of age were divided into 2 groups receiving either water alone (control) or 5% (w/v^{-1}) DSS (40,000–50,000 MW; USB Corp.) in water ad libitum for 7 days. Mice were checked daily for development of colitis by monitoring body weight, fecal occult blood (One-Step; Henry Schein Inc.) or gross rectal bleeding, and stool consistency. The overall disease severity was assessed by a clinical scoring system with a scale of 0–4, as per ref. 46. In brief, scoring was as follows: 0, no weight loss, no occult blood in the stools, and normal stool consistency; 1, weight loss of 1–5%, no occult blood, and normal stool consistency; 2, 5–10% weight loss, positive for fecal occult blood, and loose stools; 3, 10–20% weight loss, positive for fecal occult blood, and loose stools; and 4, greater than 20% weight loss, gross (visible) rectal bleeding, and diarrhea (loose stools with perianal soiling).

Animals were sacrificed by inhalational isoflurane (Baxter) overdose on day 8. The colon was removed from its mesentery to the pelvic brim and equally divided into proximal and distal segments before it was opened longitudinally. The tissues were then fixed in 4% formaldehyde (Fisher Scientific International) overnight and transferred to 70% ethanol. After embedding in paraffin, longitudinal sections of the entire colon were prepared for histological studies. Mucosal injury was assessed under high power (×200). Each field encompassed a circular area of 0.07 mm^2. The method of crypt scoring by Murthy et al. (22) was used, with the entire colon assessed. In brief, scoring was a follows: 0, normal morphology; 1, loss of lower third of the crypt; 2, loss of lower two-thirds of the crypt; 3, loss of entire crypt but with remaining surface epithelium; and 4, loss of entire glands and epithelium. Each field was assigned a grade of 0 to 4. The changes were quantitated according to the percentage involvement of the disease process: 1, 1–25%; 2, 26–50%; 3, 51–75%; and 4, 76–100% of area examined. Each field was scored with a grade and percentage area of involvement, and the product of the two was the crypt score for that field. The scores from all fields in a segment of colon were summed, which yielded a crypt score for that segment of the colon. A modified grading scale of Egger et al. (24) and Okayasu et al. (23) was also used to assess the microscopic mucosal injury in each field. The entire colon was assessed. In brief, scores were determined as follows: 0, normal morphology; 1, focal inflammatory cell infiltrate around the crypt base; 2, diffuse infiltration of inflammatory cells around crypts or erosion/destruction of lower one-third of the gland; 3, erosion/destruction of lower two-thirds or loss of all glands but with remaining surface epithelium; and 4, loss of the entire glands and epithelium. Each field was assigned a grade of 0 to 4. The total number of fields demonstrating each injury grade was quantified and expressed as a percentage of the total number of fields in the longitudinal section of the colon for each mouse (no. of fields graded 0, 1, 2, 3, or 4/total fields examined).

Analysis of intestinal morphometrics, proliferation, and apoptosis. Histological sections were prepared and stained by the Morphology Core of the Washington University Digestive Diseases Research Core Center. Routine H&E staining was performed on paraffin-embedded tissues for morphometric analyses as previously described (47, 48). Villus heights, crypt depths, and crypt cell numbers were measured in all intestinal segments in at least 10 well-oriented, full-length crypt-villus units. Quantitative analyses were performed by AxioVision analysis of digitally acquired images (version 2; Zeiss). Quantification of crypt fission was expressed as the number of crypts undergoing fission per 100 crypts counted. A crypt undergoing fission was defined as a bifurcating crypt with a bisecting fissure as illustrated in Figure 4, B and C, and per ref. 19. Crypt cell proliferation was measured by quantifying 5-BrdU incorporation into DNA, as previously described (48). Mice were injected intraperitoneally with a solution of 5-bromodeoxyuridine (8 g/l) and 5-fluorodeoxyuridine (0.8 g/l), total dose 120 mg/kg, and were sacrificed 90 minutes after injection. 5-BrdU was detected with a monoclonal anti-BrdU antibody (Zymed Laboratories Inc.) and streptavidin-biotin amplification. Crypt cell proliferation was expressed as the percentage of 5-BrdU–labeled cells per 100 crypt cells. For colitis experiments, crypt cell proliferation was assessed by quantifying 5-BrdU–labeled cells in all full-length crypts in the longitudinal sections of colons. At least 20 full-length crypts per sample were counted. Crypt cell proliferation indices were also quantified separately in areas adjacent to ulcerations and were compared with each other in WT and *epimorphin*$^{-/-}$ mice. Quantification of apoptotic cells was performed by morphologic assessment of tissues stained with H&E, as previously described (48). The number of apoptotic cells per crypt and per 1000 crypt cells was measured.

Immunoblot analyses. Protein extracts were prepared from small intestine, colon, kidney, liver, lung, brain, and testis, and 100 μg aliquots were electrophoresed on 10% SDS-polyacrylamide gels and transferred onto PVDF-plus membranes. Nuclear and cytoplasmic/membrane protein preparations were performed as follows: intestines were homogenized in Tris buffer containing 20 mM Tris-HCl, 2 mM EDTA, 10 mM EGTA, and 0.25 M sucrose and proteinase inhibitors and centrifuged at 100 *g* for 10 minutes. The pellet was discarded and the remaining supernatant centrifuged at 400 *g*. The pellet was discarded again, and the supernatant was

recentrifuged at 1,500 *g*. Supernatant was saved for cytosolic/membrane protein isolation. Nuclear protein was extracted from the pellet using homogenization buffer plus Triton X-100 (0.2%), which was mixed vigorously and centrifuged at 4°C at 15,000 *g* for 1 hour. Nuclear proteins were contained in the supernatant. Immunoblots were incubated with a rabbit polyclonal anti-epimorphin/syntaxin 2 antibody (1:2000; gift from B. Quinones, University of California Berkeley, Berkeley, California, USA, and Mark K. Bennett, Chiron Corp., Emeryville, California, USA; ref. 18), rabbit polyclonal anti–syntaxin 4 (1:1000; Synaptic Systems), mouse monoclonal anti–syntaxin 1 (1:1000; Synaptic Systems), rabbit polyclonal anti–β-catenin antibody (1:1000; Cell Signaling Technology), or mouse monoclonal anti-actin antibody (1:1000; Chemicon International) to control for differences in total protein loading or mouse monoclonal anti-lamin B1 antibody (1 μg/ml; Zymed Laboratories Inc.) to control for differences in nuclear protein loading, followed by a horseradish peroxidase–conjugated anti-IgG antibody (1;1000–1:10,000; Amersham Biosciences), and developed with chemiluminescent peroxidase substrate (ECL Western Blotting Kit; Amersham Biosciences). Relative abundance of β-catenin and lamin B1 proteins were quantified by NIH Image 1.6 analysis of digitized images of the specific bands (http://rsb.info.nih.gov/nih-image/), obtained with a UMAX Powerlook 1100 scanner using UMAX MagicScan, version 4.4.

Quantitative real-time RT-PCR. Total RNA from proximal jejunum was extracted by TriReagent (Sigma-Aldrich). The RNAs were treated with DNase I using the DNA-free kit (Ambion Inc.). First strand cDNA was synthesized from 1 μg of total RNA using SuperScript II Reverse Transcriptase (Invitrogen Corp.) with random hexamer primers (Invitrogen Corp.). Real-time RT-PCR analysis was performed on SDS 7000 (Applied Biosystems) using 2× SYBR Green Master Mix (Applied Biosystems). Oligonucleotide primers were chosen using Primer Express software (version 2.0; Applied Biosystems). Primers used in quantitative RT-PCR were as follows: cyclin D1, forward 5′-CCTTGACTGCCGAGAAGTTGT-3′ and reverse 5′-TGTTCACCAGAAGCAGTTCCAT-3′; Bmp2, forward 5′-CCAAAATCCCTAAGGCATGCT-3′ and reverse 5′-TTCATTTTCATC-TAGGTACAACATGGA-3′; Bmp4, forward 5′-TGGGCTGGAATGATTG-GATT-3′ and reverse 5′-CAGTCCCCATGGCAGTAGAAG-3′; 18s ribosomal RNA, forward 5′-CGGCTACCACATCCAAGGAA-3′ and reverse 5′-GCTGGAATTACCGCGGCT-3′; mIFN-γ, forward 5′-GGCAAGC-CAAGATCTCAGTCA-3′ and reverse 5′-CCACGGCCCCCATACA-3′; mIL-1β, forward 5′-TCGCTCAGGGTCACAAGAAA-3′ and reverse 5′-CATCAGAGGCAAGGAGGAAAAC-3′; iNOS, forward 5′-TGACGGCAAA-CATGACTTCAG-3′ and reverse 5′-GCCATCGGGCATCTGGTA-3′; Cox-2, forward 5′-CATCCCAGGCCGACTAAATG-3′ and reverse 5′-TTTCAGAG-CATTGGCCATAGAA-3′; TNF-α, forward 5′-TACCTTGTCTACTCCCAG-GTTCTCT-3′ and reverse 5′-GTGTGGGTGAGGAGCACGTA-3′; IL-6, forward 5′-CTTCCTACCCCAATTTCCAATG-3′ and reverse 5′-ATTGGAT-GGTCTTGGTCCTTAGC-3′.

For all primer sets, the kinetics of the PCR was confirmed by serial dilutions of different cDNA preparations. These analyses verified that the efficiencies of amplification were equal for both primer sets and thereby allowing quantification by the comparative Ct method (49).

Epimorphin transfected myofibroblast–Caco-2 cell grafts in nude mice. The full-length epimorphin/syntaxin 2 cDNA was cloned and transfected into Mic216 intestinal myofibroblasts in sense and antisense orientations as in ref. 15. Levels of epimorphin were quantified by immunoblot. Epimorphin expression was inhibited in antisense-transfected cells and was 3- to 4-fold overexpressed in sense-transfected cells (15). The transfected myofibroblasts were cocultured with epithelial Caco-2 cells for 2 days in DMEM medium containing 20% FCS, 1% nonessential amino acids, 1% penicillin, and 1% streptomycin, then were harvested and injected into the subcutaneous tissue of nude mice. Tumors were removed 6 weeks after grafting. Tumors were fixed in formalin, paraffin embedded, and sectioned in preparation for Bmp immunohistochemical analyses as detailed above.

Bmp4 treatment of epimorphin antisense-transfected myofibroblast–Caco-2 cell cocultures. Caco-2 cells were cocultured with epimorphin-antisense–transfected myofibroblasts for 5 days as described above. Cocultures were exposed to either control media plus vehicle (4 mM HCl plus 0.1% BSA) or media containing Bmp4 dissolved in vehicle (100–200 ng/ml; R&D Systems). Bmp4 was added at the time of plating and then daily for 5 days.

Statistics. Means were compared between WT and KO mice using 2-tailed Student's *t* test (Microsoft Excel 2003). Values in the text are means ± SEM. Differences were considered significant at $P < 0.05$.

Acknowledgments

We thank Renu Singh for her excellent technical assistance, Ted Simon and David Ornitz for their help in generating the epimorphin$^{-/-}$ mice, Randy May and Karen Hutton for help with general immunostaining protocols, and Filipe Muhale for his help with β-catenin immunostaining. These studies were supported by NIH National Institute of Diabetes and Digestive and Kidney Diseases grants DK61216 (to D.C. Rubin), DK46122 (to D.C. Rubin), DK50466 (to M.S. Levin), and DK52574; the Morphology Core and Murine Models Core of the Digestive Diseases Research Core Center of the Washington University School of Medicine; and the Embryonic Stem Cell Core of the Siteman Cancer Center at Washington University School of Medicine.

Received for publication April 22, 2005, and accepted in revised form March 28, 2006.

Address correspondence to: Deborah C. Rubin, Division of Gastroenterology, Washington University School of Medicine, 660 South Euclid Avenue, Box 8124, St. Louis, Missouri 63110, USA. Phone: (314) 362-8935; Fax: (314) 362-8959; E-mail: drubin@wustl.edu.

1. Kedinger, M., Lefebvre, O., Duluc, I., Freund, J.N., and Simon-Assmann, P. 1998. Cellular and molecular partners involved in gut morphogenesis and differentiation. *Philos. Trans. R. Soc. Lond. B. Biol. Sci.* **353**:847–856.
2. de Santa Barbara, P., van den Brink, G.R., and Roberts, D.J. 2003. Development and differentiation of the intestinal epithelium. *Cell. Mol. Life Sci.* **60**:1322–1332.
3. Walters, J.R. 2004. Cell and molecular biology of the small intestine: new insights into differentiation, growth and repair. *Curr. Opin. Gastroenterol.* **20**:70–76.
4. Perreault, N., Katz, J.P., Sackett, S.D., and Kaestner, K.H. 2001. Foxl1 controls the Wnt/beta-catenin pathway by modulating the expression of proteoglycans in the gut. *J. Biol. Chem.* **276**:43328–43333.
5. Haramis, A.P., et al. 2004. De novo crypt formation and juvenile polyposis on BMP inhibition in mouse intestine. *Science.* **303**:1684–1686.
6. Madison, B.B., et al. 2005. Epithelial hedgehog signals pattern the intestinal crypt-villus axis. *Development.* **132**:279–289.
7. Hirai, Y., et al. 1998. Epimorphin functions as a key morphoregulator for mammary epithelial cells. *J. Cell Biol.* **140**:159–169.
8. Mori, M., and Miyazaki, K. 2000. Factors affecting morphogenesis of rabbit gallbladder epithelial cells cultured in collagen gels. *Cell Tissue Res.* **300**:331–344.
9. Lehnert, L., et al. 2001. Autocrine stimulation of human pancreatic duct-like development by soluble isoforms of epimorphin in vitro. *J. Cell Biol.* **152**:911–922.
10. Hirai, Y., et al. 2001. Epimorphin mediates mammary luminal morphogenesis through control of C/EBPbeta. *J. Cell Biol.* **153**:785–794.
11. Miura, K., et al. 2003. Epimorphin is involved in differentiation of rat hepatic stem-like cells through cell-cell contact. *Biochem. Biophys. Res. Commun.* **311**:415–423.
12. Radisky, D.C., Hirai, Y., and Bissell, M.J. 2003. Delivering the message: epimorphin and mammary epithelial morphogenesis. *Trends Cell Biol.* **13**:426–434.
13. Goyal, A., Singh, R., Swietlicki, E.A., Levin, M.S., and Rubin, D.C. 1998. Characterization of rat epimorphin/syntaxin 2 expression suggests a role in

crypt-villus morphogenesis. *Am. J. Physiol. Gastrointest. Liver Physiol.* **38**:G114–G124.
14. Plateroti, M., et al. 1998. Subepithelial fibroblast cell lines from different levels of gut axis display regional characteristics. *Am. J. Physiol.* **274**:G945–G954.
15. Fritsch, C., et al. 2002. Epimorphin expression in intestinal myofibroblasts induces epithelial morphogenesis. *J. Clin. Invest.* **110**:1629–1641. doi:10.1172/JCI200213588.
16. Goyal, A., Singh, R., Swietlicki, E.A., Levin, M.S., and Rubin, D.C. 1998. Characterization of rat epimorphin/syntaxin 2 expression suggests a role in crypt-villus morphogenesis. *Am. J. Physiol.* **275**:G114–G124.
17. Bennett, M.K., et al. 1993. The syntaxin family of vesicular transport receptors. *Cell.* **74**:863–873.
18. Quinones, B., Riento, K., Olkkonen, V.M., Hardy, S., and Bennett, M.K. 1999. Syntaxin 2 splice variants exhibit differential expression patterns, biochemical properties and subcellular localizations. *J. Cell Sci.* **112**:4291–4304.
19. He, X.C., et al. 2004. BMP signaling inhibits intestinal stem cell self-renewal through suppression of Wnt-beta-catenin signaling. *Nat. Genet.* **36**:1117–1121.
20. Strober, W., Fuss, I.J., and Blumberg, R.S. 2002. The immunology of mucosal models of inflammation. *Annu. Rev. Immunol.* **20**:495–549.
21. Pull, S.L., Doherty, J.M., Mills, J.C., Gordon, J.I., and Stappenbeck, T.S. 2005. Activated macrophages are an adaptive element of the colonic epithelial progenitor niche necessary for regenerative responses to injury. *Proc. Natl. Acad. Sci. U. S. A.* **102**:99–104.
22. Murthy, S.N., et al. 1993. Treatment of dextran sulfate sodium-induced murine colitis by intracolonic cyclosporin. *Dig. Dis. Sci.* **38**:1722–1734.
23. Okayasu, I., et al. 1990. A novel method in the induction of reliable experimental acute and chronic ulcerative colitis in mice. *Gastroenterology.* **98**:694–702.
24. Egger, B., et al. 1998. Reduced susceptibility of mice overexpressing transforming growth factor alpha to dextran sodium sulphate induced colitis. *Gut.* **43**:64–70.
25. Andoh, A., Fujino, S., Hirai, Y., and Fujiyama, Y. 2004. Epimorphin expression in human colonic myofibroblasts. *Int. J. Mol. Med.* **13**:57–61.
26. Powell, D.W., et al. 1999. Myofibroblasts. II. Intestinal subepithelial myofibroblasts. *Am. J. Physiol.* **277**:C183–C201.
27. Powell, D.W., et al. 1999. Myofibroblasts. I. Paracrine cells important in health and disease. *Am. J. Physiol.* **277**:C1–C9.
28. Brittan, M., and Wright, N.A. 2004. The gastrointestinal stem cell. *Cell Prolif.* **37**:35–53.
29. Hirai, Y. 2001. Epimorphin as a morphogen: does a protein for intracellular vesicular targeting act as an extracellular signaling molecule? *Cell Biol. Int.* **25**:193–195.
30. St. Clair, W.H., and Osborne, J.W. 1985. Crypt fission and crypt number in the small and large bowel of postnatal rats. *Cell Tissue Kinet.* **18**:255–262.
31. Bascom, J.L., Fata, J.E., Hirai, Y., Sternlicht, M.D., and Bissell, M.J. 2005. Epimorphin overexpression in the mouse mammary gland promotes alveolar hyperplasia and mammary adenocarcinoma. *Cancer Res.* **65**:8617–8621.
32. Kitajima, S., Takuma, S., and Morimoto, M. 1999. Changes in colonic mucosal permeability in mouse colitis induced with dextran sulfate sodium. *Exp. Anim.* **48**:137–143.
33. Mashimo, H., Wu, D.-C., Podolsky, D.K., and Fishman, M.C. 1996. Impaired defense of intestinal mucosa in mice lacking intestinal trefoil factor. *Science.* **274**:262–265.
34. Beck, P.L., et al. 2003. Transforming growth factor-beta mediates intestinal healing and susceptibility to injury in vitro and in vivo through epithelial cells. *Am. J. Pathol.* **162**:597–608.
35. Fiocchi, C. 1997. Intestinal inflammation: a complex interplay of immune and nonimmune cell interactions. *Am. J. Physiol.* **273**:G769–G775.
36. Di Mari, J.F., Mifflin, R.C., Adegboyega, P.A., Saada, J.I., and Powell, D.W. 2003. IL-1alpha-induced COX-2 expression in human intestinal myofibroblasts is dependent on a PKCzeta-ROS pathway. *Gastroenterology.* **124**:1855–1865.
37. Otte, J.M., Rosenberg, I.M., and Podolsky, D.K. 2003. Intestinal myofibroblasts in innate immune responses of the intestine. *Gastroenterology.* **124**:1866–1878.
38. van Tol, E.A., et al. 1999. Bacterial cell wall polymers promote intestinal fibrosis by direct stimulation of myofibroblasts. *Am. J. Physiol.* **277**:G245–G255.
39. Hackam, D.J., et al. 1996. Characterization and subcellular localization of target membrane soluble NSF attachment protein receptors (t-SNAREs) in macrophages. Syntaxins 2, 3, and 4 are present on phagosomal membranes. *J. Immunol.* **156**:4377–4383.
40. Pagan, J.K., et al. 2003. The t-SNARE syntaxin 4 is regulated during macrophage activation to function in membrane traffic and cytokine secretion. *Curr. Biol.* **13**:156–160.
41. Murray, R.Z., Wylie, F.G., Khromykh, T., Hume, D.A., and Stow, J.L. 2005. Syntaxin 6 and Vti1b form a novel SNARE complex, which is up-regulated in activated macrophages to facilitate exocytosis of tumor necrosis factor-alpha. *J. Biol. Chem.* **280**:10478–10483.
42. Kierszenbaum, A.L. 2000. Fusion of membranes during the acrosome reaction: a tale of two SNAREs. *Mol. Reprod. Dev.* **57**:309–310.
43. Katafuchi, K., Mori, T., Toshimori, K., and Iida, H. 2000. Localization of a syntaxin isoform, syntaxin 2, to the acrosomal region of rodent spermatozoa. *Mol. Reprod. Dev.* **57**:375–383.
44. Ge, R.S., et al. 2005. Gene expression in rat leydig cells during development from the progenitor to adult stage: a cluster analysis. *Biol. Reprod.* **72**:1405–1415.
45. Qin, J., et al. 2005. Regulation of embryo outgrowth by a morphogenic factor, epimorphin, in the mouse. *Mol. Reprod. Dev.* **70**:455–463.
46. Castagliuolo, I., et al. 2002. Protective effects of neurokinin-1 receptor during colitis in mice: role of the epidermal growth factor receptor. *Br. J. Pharmacol.* **136**:271–279.
47. Rubin, D.C., Swietlicki, E.A., Wang, J.L., and Levin, M.S. 1998. Regulation of PC4/TIS7 expression in adapting remnant intestine post-resection. *Am. J. Physiol.* **275**:G506–G513.
48. Tang, Y., et al. 2004. Bax is required for resection-induced changes in apoptosis, proliferation, and members of the extrinsic cell death pathways. *Gastroenterology.* **126**:220–230.
49. Applied Biosystems. 1997. ABI Prism 7700 Sequence Detection System. User bulletin #2. http://docs.appliedbiosystems.com/pebiodocs/04303859.pdf.